Received: 6 March 2025 | Revised: 27 May 2025 | Accepted: 16 June 2025

DOI: 10.1111/bph.70133

RESEARCH ARTICLE

Structure-based discovery of thiamine uptake inhibitors

Florian Gabriel[1,2] | Björn Windshügel[3,4] | Christian Löw[1,2,5]

[1]Centre for Structural Systems Biology (CSSB), Hamburg, Germany

[2]European Molecular Biology Laboratory (EMBL) Hamburg, Hamburg, Germany

[3]Fraunhofer Institute for Translational Medicine and Pharmacology ITMP, Discovery Research ScreeningPort, Hamburg, Germany

[4]School of Science, Constructor University, Bremen, Germany

[5]Bernhard Nocht Institute for Tropical Medicine, Hamburg, Germany

Correspondence
Björn Windshügel, Fraunhofer Institute for Translational Medicine and Pharmacology ITMP, Discovery Research ScreeningPort, 22525 Hamburg, Germany.
Email: bjoern.windshuegel@itmp.fraunhofer.de

Christian Löw, European Molecular Biology Laboratory Hamburg, Notkestrasse 85, D-22607 Hamburg, Germany.
Email: christian.loew@embl-hamburg.de
Twitter handle: @AllUNeedIsLoew

Background and Purpose: Thiamine (vitamin B_1) is an essential coenzyme and catalyses various reactions in central metabolic pathways. Since mammals have lost the ability to synthesise thiamine de novo, this micronutrient has to be imported via the high affinity solute carriers SLC19A2 and A3 across the plasma membrane. Perturbations of these transport systems have severe effects on human health. Recent structural work on SLC19A2 and A3 have provided molecular insights into substrate and drug recognition and conformational changes during transport. Based on the analysis of the available SLC19A3 structures, we hypothesise that the binding site is rather promiscuous, allowing different small molecules to interact and potentially inhibit this transporter.

Experimental Approach: We employed a computational approach, by which 538 approved and investigational drugs were docked into an ensemble of SLC19A3 cryo-EM structures, followed by experimental binding studies, transport inhibition assays, and structural validation.

Key Results: Eight novel compounds were identified that bind and inhibit SLC19A3. To visualise such a new drug interaction, we determined the cryo-EM structure of SLC19A3 bound to domperidone, a dopamine D_2 receptor antagonist used for the treatment of nausea and gastrointestinal disorders. Our computational work together with biochemical and cellular transport assays expands the understanding of SLC19A3-drug interactions, highlights the power of virtual screening approaches using structural ensembles, and provides a three-dimensional pharmacophore model for SLC19A3 inhibitors.

Conclusion and Implications: These findings offer a basis for addressing drug-induced thiamine deficiencies and pre approach can be used to optimise pharmacological strategies involving SLC19A3-interacting compounds in the future.

KEYWORDS
cryo-EM structure, inhibitor, SLC19A3, thiamine uptake, virtual screening

Abbreviations: ChemPLP, chemical piecewise linear potential; CHS, cholesteryl hemisuccinate; Cryo-EM, cryo-Electron Microscopy; CTD, C-terminal domain; HBD, hydrogen bond donor; hERG, human ether-a-go-go-related gene; LMNG, lauryl maltose neopentyl glycol; MFS, Major Facilitator Superfamily; MFSD1, major facilitator superfamily domain-containing protein 1; MOE, Molecular Operating Environment; nanoDSF, nano-Differential Scanning Fluorimetry; NTD, N-terminal domain; Nb3.3, nanobody 3.3; RMSD, root mean square deviation; TCEP, tris (2-carboxyethyl)phosphine; thiamine-pp, thiamine pyrophosphate; TPK1, thiamine pyrophosphokinase; TPSA, topological surface area; TUI, thiamine uptake inhibitors; VS, virtual screening; WLE, Wernicke's-like encephalopathy.

1 | INTRODUCTION

Thiamine (vitamin B_1) is essential for cell survival and an important micronutrient for humans and other mammals (Manzetti et al., 2014). Inside cells, it is converted to thiamine pyrophosphate (thiamine-pp) by the thiamine pyrophosphokinase 1 (TPK1) (Baker et al., 2001; Timm et al., 2001). Thiamine-pp functions as a coenzyme in crucial metabolic processes such as the citric acid cycle and the pentose phosphate pathway (Tylicki et al., 2018). Due to the inability of mammals to synthesise thiamine de novo, its uptake depends on specific transporters located in the plasma membrane. Among these, the solute carrier family members **SLC19A2** and **SLC19A3** are high-affinity thiamine transporters that facilitate the vitamin's entry into cells (Dutta et al., 1999; Rajgopal et al., 2001; Zhao & Goldman, 2013). SLC19A3 is especially important for thiamine transport across the intestinal wall and blood–brain barrier, with mutations leading to severe pathological conditions such as Wernicke's-like encephalopathy (WLE) and biotin- and thiamine-responsive basal ganglia disease (Alfadhel et al., 2019; Kono et al., 2009; Wang et al., 2021; Wen et al., 2023; Zeng et al., 2005). This underscores the physiological importance of SLC19A3 in maintaining thiamine homeostasis. SLC19A3 has been implicated in several drug interactions, including several antidepressants, antibiotics, and antineoplastic drugs inhibiting thiamine uptake by this transporter. The **JAK** inhibitor **fedratinib**, for example, has been linked to the development of Wernicke's encephalopathy due to its high-affinity inhibition of SLC19A3 (Pardanani et al., 2015; Zhang et al., 2014).

Recently, the structures of SLC19A3 and A2 in their apo and thiamine-bound states have been determined (Dang et al., 2024; Gabriel et al., 2024; Li et al., 2024). These Major Facilitator Superfamily (MFS) transporters function through the alternating access mechanism (Drew et al., 2021; Jardetzky, 1966; Quistgaard et al., 2016), whereby conformational changes facilitate substrate binding, translocation and release. The use of different fiducial markers for cryo-EM analysis trapped the vitamin transporters in different conformations and revealed detailed molecular insights in associated conformational changes during transport. Structures of SLC19A3 in complex with known thiamine uptake inhibitors (TUI) showed that the substrate binding site of the transporter is rather promiscuous and not selective for thiamine, indicating that a potentially larger pool of small molecules would be able to block thiamine uptake via SLC19A3 and, probably, also SLC19A2.

To test this hypothesis, we combined a computational docking approach of approved and investigational drug molecules with binding and transport-inhibition experiments and determined the cryo-EM structure of SLC19A3 bound to **domperidone**, a dopamine **D_2 receptor** antagonist commonly used to treat nausea and gastrointestinal disorders. Our computational work together with biochemical and cellular transport assays expands the understanding of SLC19A3-drug interactions and highlights the implications of domperidone-mediated transporter inhibition. These findings may inform future strategies for mitigating drug-induced thiamine deficiencies and optimising pharmacological interventions involving SLC19A3-interacting compounds.

What is already known

- Cryo-EM structures of the thiamine transporters SLC19A2 and SLC19A3
- Thiamine uptake via SLC19A3 can be inhibited by the JAK inhibitor fedratinib

What does this study add?

- Computational docking of a drug library to an ensemble of structures increases hit rate
- Identification of eight approved and investigational drugs inhibiting SLC19A3

What is the clinical significance?

- Drug interactions affecting SLC19A3 may have severe consequences in populations at risk for thiamine deficiencies
- Molecular docking to evaluate transporter binding systematically in drug safety assessments

2 | METHODS

2.1 | Molecular modelling

The screening library was based on the SCREEN-WELL® FDA approved drug library (Enzo Biochem Inc., Farmingdale, NY, USA). Altogether 538 approved and investigational drugs were selected for the virtual screening campaign. Considering the enantiomeric forms of substances with chiral centres, we assessed a total of 722 structures. Cryo-EM structures of unliganded SLC19A3 and the protein-ligand complexes containing either thiamine, fedratinib, amprolium, **hydroxychloroquine**, or **amitriptyline** were superposed using Molecular Operating Environment (MOE) version 2022.02 and prepared in presence of the bound ligands (protonation, hydrogen bond network optimisation) with Protonate3D in MOE (Chemical Computing Group Inc., Montreal, Canada). Initially, the five SLC19A3-bound compounds were re-docked into the cryo-EM structures utilising 3D structures retrieved from PubChem to avoid any bias by using starting coordinates of bound ligands.

Molecular docking was carried out using GOLD version 2023.3.0 (Cambridge Crystallographic Data Centre, Cambridge, UK) and the default scoring function ChemPLP. For each compound 50 docking runs were conducted. The early termination option was switched off. All compounds were docked into a sphere of 12 Å radius centred on the C4 atom of thiamine (PDB ID: 8S61). Binding

modes of top-ranked compounds were visually inspected using MOE. The conformation database for the pharmacophore search was generated by a stochastic search within MOE using default settings except for the iteration limit (1000) and the MM iteration limit (200). MOE was used for pharmacophore modelling and molecular descriptor calculation.

2.2 | Expression and purification of SLC19A3

The cDNA of SLC19A3 (Uniprot accession number: Q9BZV2) was cloned into a pXLG vector, fusing the transporter with a C-terminal Twin-Strep tag, connected by an HRV 3C cleavage site and a flexible GSSG linker. Plasmid DNA was produced at large scale in *E. coli* DH5α and extracted and purified using the NucleoBond PC 10000 EF Giga Kit (Macherey-Nagel). For overexpression of SLC19A3, the expression vector was transfected in log-phase Expi293F™ cells (RRID: CVCL_D615) using PEI MAX® as transfection reagent. Transfection was performed by incubating Expi293F™ cells at a density of 20 x 10^6 cells ml^{-1} with 30 ng ml^{-1} plasmid DNA and 60 ng ml^{-1} PEI MAX® for 45 min at 37 °C, 8% (v/v) CO_2, and 270 rpm in FreeStyle™ medium. The cells were subsequently diluted to 2 x 10^6 cells ml^{-1} with fresh FreeStyle™ medium and grown for 96 hours to allow for sufficient overexpression of the transfected constructs. Afterwards, cells were harvested for 5 min at 3,000 × g (22°C) and washed with 1 × PBS (pH 7.4). Cell pellets were frozen and stored at −70 °C. The overexpressed SLC19A3 was extracted using whole cell solubilisation with a detergent mixture of lauryl maltose neopentyl glycol (LMNG) and cholesteryl hemisuccinate (CHS). For this, 5 g of frozen cell pellet were thawed in a water bath at room temperature and subsequently resuspended in 25 ml of solubilisation buffer (1 × PBS, pH 7.4, 200 mM NaCl, 5% glycerol (v/v), 1% LMNG, 0.1% CHS, 1 × EDTA-free protease inhibitors, 0.5 mM tris(2-carboxyethyl)phosphine (TCEP), 20 U ml^{-1} DNase I, 2.5 U avidin). The suspension was then incubated for 1 hour at 4 °C on a roller platform. Insoluble debris were subsequently pelleted by centrifugation for 30 min at 35,000 × g at 4 °C. The cleared supernatant was loaded on 1 ml StrepTactin resin equilibrated in StrepA buffer (20 mM Tris–HCl, pH 7.4, 350 mM NaCl, 5% glycerol (v/v), 0.5 mM TCEP, 0.02% LMNG (w/v), 0.002% CHS (w/v)). The slurry of lysate and resin was incubated for 1 hour at 4 °C to allow for quantitative binding of the Strep-tagged SLC19A3 to the StrepTactin resin. Afterwards, the slurry was loaded on a gravity column. The flow-through was discarded, and the resin was washed four times with 20 column volumes of StrepA buffer. SLC19A3 was then eluted with 5 column volumes StrepB buffer (20 mM Tris–HCl, pH 7.4, 150 mM NaCl, 0.002% LMNG, 0.0002% CHS, 10 mM desthiobiotin, pH adjusted to 7 with 1 M NaOH). The eluted protein was concentrated to 0.5 ml using a molecular weight cut-off of 50 kDa and was subsequently subjected to size-exclusion chromatography (SEC). SEC was performed in TBS-D buffer (20 mM Tris–HCl, pH 7.4, 150 mM NaCl, 0.002% LMNG, 0.0002% CHS) on a Superdex S200 10/300 Increase column (Cytiva) using an ÄKTA pure system.

2.3 | Expression and purification of the nanobody Nb3.3

Nanobody Nb3.3, cloned into the pMESy4 plasmid, was produced by overexpression in *E. coli* WK6 cells. Precultures of Nb3.3-transformed *E. coli* WK6 were grown in LB medium containing 100 μg ml^{-1} ampicillin and 2% glucose (w/v). For large-scale nanobody production, these precultures were inoculated in 1 l TB medium containing 100 mg μg ml^{-1} ampicillin and 0.1% glucose. The cells were grown for about 3–4 hours at 37 °C, shaking at 165 rpm. At an OD_{600} of 0.8–1.0, overexpression of the nanobody was induced with 1 mM IPTG. The expression cultures were then grown overnight at 22 °C, shaking at 165 rpm. Cells were subsequently harvested by centrifugation for 15 min at 12,000 × *g* (22°C). Cell pellets were frozen and stored at −70 °C. For periplasmic extraction of the overexpressed Nb3.3, 10–20 g of cell pellet were thawed in a 35 °C water bath and resuspended in 200 ml periplasmic extraction buffer (20% sucrose (w/v), 50 mM Tris–HCl, pH 7.4, 0.5 mM EDTA, pH 8.0, 1 × EDTA-free protease inhibitors, 0.5 μg ml^{-1} lysozyme, 0.5 mM TCEP). The suspension was stirred for 30 minutes at 4 °C. Afterwards, 400 ml of Mg buffer (20 mM Tris–HCl, pH 7.4, 350 mM NaCl, 1 mM $MgCl_2$, 0.5 mM TCEP) were added. Cell debris were subsequently separated by centrifugation. The soluble supernatant containing the nanobody was transferred to a fresh bottle and supplied with 1 ml Ni-NTA resin, equilibrated in HisA buffer (20 mM Tris–HCl, pH 7.4, 350 mM NaCl, 20 mM imidazole, pH 7.4). After 1 hour of incubation on a stirring platform, the suspension was loaded on a gravity column. The flow-through was discarded, and the resin washed with 4 × 20 ml of HisA buffer. The immobilised Nb3.3 was eventually eluted with 5 ml of HisB buffer (20 mM Tris–HCl, pH 7.4, 350 mM NaCl, 400 mM imidazole, pH 7.4, 0.5 mM TCEP). The elution was then concentrated to 0.5 ml using a 10 kDa molecular weight cut-off concentrator and subjected to size-exclusion chromatography on a Superdex S75 10/300 Increase column in TBS buffer (20 mM Tris HCl, pH 7.4, 150 mM NaCl) on an AKTA Pure system. Protein samples were analysed by SDS-PAGE. The purified nanobody was concentrated using 10 kDa molecular weight cut-off concentrators, flash-frozen in liquid nitrogen, and stored at −70 °C.

2.4 | Thermal stabilisation assays (nanoDSF)

The thermal stabilisation of SLC19A3 by small molecule drugs was assessed using nanoDSF on a Prometheus NT.48 instrument (NanoTemper Technologies). For sample preparation, SLC19A3 was diluted to a final concentration of 4 μM in TBS-D buffer (20 mM Tris–HCl, pH 7.4, 150 mM NaCl, 0.002% LMNG (w/v) and 0.0002% CHS (w/v)) containing the respective drug. Compounds for initial hit validation were taken from compound collections at Fraunhofer ITMP: carbamylcholine, 4-amino-salicylic-acid, and sotalol were taken from the SCREEN-WELL® FDA approved drug library V2 (Enzo Biochem Inc., Farmingdale, NY, USA), all other compounds were taken from the Fraunhofer Repurposing Collection, assembled by Specs, Zoetermeer,

Netherlands. For apparent binding affinity determination, domperidone (# 18875, Cayman Chemical, Ann Arbor, MI, USA) was obtained from Cayman Chemical, Ann Arbor, MI.

Prior to nanoDSF measurements, samples were incubated for 30 minutes at room temperature to allow for a steady-state binding equilibrium to be established. Melting scans were performed over a temperature range from 20 to 95 °C, with a temperature increase of 1 °C per minute. Thermal unfolding was monitored by measuring the fluorescence of the protein's tryptophan residues at 350 nm (F350) and 330 nm (F330). Thermal unfolding curves were commonly based on F350. The protein melting temperature (T_m) was identified as the inflection point of the thermal unfolding curve, which corresponds to the local maximum or minimum of its first derivative. The melting scan data were analysed using the manufacturer's software (PR.ThermControl, v 2.1.2, NanoTemper Technologies). Ligand-induced thermal shifts (ΔT_m) were calculated as the difference between the melting temperatures of the ligand-bound state (T_m) and the apo state (T_m^{apo}) of SLC19A3. To determine apparent binding affinities of ligands at 25 °C, T_m values from dilution series of the respective small molecule compounds were used to fit the parameters of the following equation (Equation 1).

$$\frac{\Delta T_m}{T_m^{apo}}(L) = \frac{-RT_{std}}{E_{a1}} * \ln\left(\frac{K_{d,app}}{K_{d,app}+L}\right) \quad (1)$$

with L being the ligand concentration, R the universal gas constant, T_{std} the chosen standard temperature of 298.15 K (25 °C), and E_{a1} the activation energy for the unfolding of the apo state. As R, T_{std} and L are known and the ΔT_m and T_m^{apo} are experimentally determined, it is possible to use non-linear curve fitting to estimate E_{a1} and $K_{d,app}$. The fitting was done in symfit (v. 0.5.3), as described (Kotov et al., 2023), based on theoretical considerations formulated by Hall (Hall, 2019).

2.5 | Mass spectrometry-based cellular thiamine uptake assays

The uptake of deuterated thiamine (thiamine-d_3) by SLC19A3 and mock-transfected Expi293F™ cells was measured using LC–MS/MS. Expi293F™ cells were transfected as described above and grown for 48 hours at 37 °C, under 8% CO_2 (v/v), and shaking at 270 rpm. Thereafter, the cells were harvested by centrifugation for 5 minutes at 250 × g (22°C). For the uptake assays, the cells were resuspended at a cell density of 0.2 or 2 x 10^6 cells ml^{-1} in 1 × PBS (pH 7.4). The resulting cell suspension was subsequently aliquoted into a 96-deep well plate. The assay was set up with three independently transfected cell batches per condition ($n = 3$, 1 ml per well). Each well was supplied with 20 or 200 µM of the respective compound to be tested. The 96-well plate was then incubated for 1 minute on a shaking platform. Next, 2 µM of thiamine-d_3 were added, and the plate was incubated for an additional 5 minutes. The cells were then pelleted for 5 minutes at 500 × g and washed three times with 1 ml of 1 × PBS (pH 7.4). Finally, the cell suspensions were transferred to a fresh 96-deep well plate. The cells were pelleted, aspirated, and stored at −70 °C. For the LC–MS/MS analysis, the samples were extracted by adding 500 µl of a mixture of H_2O: MeOH: ACN (1:1:1, v/v), containing 5% formic acid. After vortexing and ultrasonication in a water bath for 5 min at 4 °C, samples were incubated for 20 min at −20 °C. Ultimately, samples were centrifuged at 15,000 × g and 4 °C for 10 minutes using a 5415R microcentrifuge (Eppendorf, Hamburg, Germany). The supernatants were then transferred for LC–MS analysis, which was initiated within one hour after sample preparation. LC–MS/MS analysis was performed on a Vanquish UHPLC system coupled to an Orbitrap Exploris 240 high-resolution mass spectrometer (Thermo Fisher Scientific, MA, USA) in positive ESI (electrospray ionisation) mode. Chromatographic separation was carried out on an Atlantis Premier BEH Z-HILIC column (Waters, MA, USA; 2.1 mm x 100 mm, 1.7 µm) at a flow rate of 0.25 ml/min. The mobile phase consisted of water: acetonitrile (9:1, v/v; mobile phase A) and acetonitrile: water (9:1, v/v; mobile phase B), which were modified with a total buffer concentration of 10 mM ammonium formate. The aqueous portion of each mobile phase was adjusted to pH 3.0 via addition of formic acid. The following gradient (8 min total run time including re-equilibration) was applied (time [min]/%B): 0/90, 3/85, 3.5/60, 4/60, 5/90, 8/90. Column temperature was maintained at 40 °C, the autosampler was set to 4 °C and sample injection volume was set to 3 µl. Analytes were recorded via a full scan with a mass resolving power of 120,000 over a mass range from 60–900 *m/z* (scan time: 100 ms, RF lens: 70%). MS/MS fragment spectra were recorded via targeted product ion scans for Thiamine ($[M]^+$, $m/z = 265.1118$) and Thiamine-d_3 ($[M]^+$, $m/z = 268.1306$) at a resolving power of 15,000, stepped collision energies [%]: 20/35/50, and total cycle time of 3 sec. Ion source parameters were set to the following values: spray voltage: 3500 V, sheath gas: 30 psi, auxiliary gas: 5 psi, sweep gas: 0 psi, ion transfer tube temperature: 350 °C, vaporizer temperature: 300 °C. All experimental samples were measured in a randomised manner. Pooled quality control (QC) samples were prepared by mixing equal aliquots from each processed sample. Multiple QCs were injected at the beginning of the analysis in order to equilibrate the analytical system. A QC sample was analysed after every 6th experimental sample to monitor instrument performance throughout the sequence. For determination of background signals and subsequent background subtraction, an additional processed blank sample was recorded. Data were processed using TraceFinder 5.1 and raw peak area data was exported for relative metabolite quantification.

2.6 | Cryo-EM sample preparation and data collection

For cryo-EM, SLC19A3 was prepared in TBS-D buffer (20 mM Tris–HCl, pH 7.4, 150 mM NaCl, 0.002% LMNG (w/v), 0.0002% CHS (w/v)). The membrane transporter was concentrated to 60 µM and mixed and diluted with a 1.2-fold molar excess of Nb3.3 in TBS buffer (20 mM Tris–HCl, pH 7.4, 150 mM NaCl), resulting in final concentrations of 30 µM SLC19A3 and about 36 µM nanobody. Domperidone

(# 18875, Cayman Chemical, Ann Arbor, MI, USA) was added at a concentration of 250 μM. The cryo-EM samples were subsequently incubated on ice overnight. For the preparation of EM grids, 3.6 μl of the samples were applied to glow-discharged holey carbon film grids (Quantifoil 300 mesh, Au, R1.2/1.3) for 15 seconds at 10 °C and 100% humidity using a Vitrobot Mark IV (Thermo Fisher Scientific). Blotting was performed for 3.5 seconds with a blot force of −5 and a drain time of 0.5 seconds. The grids were then plunged into a liquid ethane/propane mixture and stored in liquid nitrogen. Cryo-EM data were collected on a Titan Krios G3 (FEI) electron microscope at the CSSB Hamburg, equipped with an X-FEG operating at 300 kV, a K3 direct electron detector camera (Gatan), and a BioQuantum imaging filter (Gatan) with a slit width set to 20 eV. The data were collected at a nominal magnification of 105,000 ×, corresponding to a pixel size of 0.83 Å, and at total doses of 60 $e^{-}/Å^2$. More details on the data collection can be found in Supplementary Table S2.

2.7 | Cryo-EM data processing

The processing of the acquired EM movies was carried out using cryoSPARC (v.4.6) (Punjani et al., 2017). The movies were first subjected to patch motion correction and CTF estimation. Motion corrected micrographs meeting high-quality criteria (CTF resolution < 3.5 Å, relative ice thickness < 1.05, total frame motion distance < 25 Å) were selected for further processing. Particle picking was performed using a template picker. The 2D references for this approach were generated from a 3D reconstruction, obtained by the processing of a small subset of the data (459 micrographs, subjected to blob-picking (100 Å blob), 2D classification, ab-initio reconstruction, and non-uniform refinement (NU-refinement)).

After template-based particle picking across the entire dataset, particles were analysed and filtered by 2D classification. The selected "good" particles were then subjected to a series of multi-class 3D ab-initio reconstructions, NU-refinements, and heterogeneous refinements to determine a first high-resolution reconstruction. The particles from this reconstruction were then subjected to local motion correction and re-extracted at larger box size of ∼326 Å (384 px). After another NU-refinement, the resulting density map was locally refined with a mask encompassing the transporter-nanobody complex but excluding the detergent micelle. Map sharpening was performed using the global Guinier plot B-factor estimates from the respective refinement jobs. For further details on EM data processing, see Supplementary Figure S2. Q-scores were calculated using the MapQ plugin in UCSF Chimera, developed by Grigore Pintilie (Pintilie et al., 2020).

2.8 | Model building and refinement

AlphaFold2 predictions were used as starting structure models for SLC19A3 and Nb3.3 (Jumper et al., 2021). The AlphaFold2 protein models were initially relaxed into the corresponding EM density maps using ISOLDE in ChimeraX (Croll, 2018; Pettersen et al., 2021). Domperidone as a ligand was built with the eLBOW package of Phenix (Afonine et al., 2018) and integrated into the protein structure model in Coot (v.0.9.8.1) (Emsley et al., 2010). The resulting model of the ternary complex underwent iterative refinement with Phenix (auto-refinement) and Coot (manual refinement). Visualisations were created using UCSF ChimeraX (v.1.4) (Pettersen et al., 2021).

2.9 | Data and statistical analysis

The data and statistical analysis comply with the recommendations of the *British Journal of Pharmacology* on experimental design and analysis in pharmacology (Curtis et al., 2022). No data points were excluded and no additional data were subjected to statistical analysis. Data were expressed as mean ± SEM. The group size (n) represents either technical or biological replicates from independent cell culture experiments, as stated. For experiments with $n < 5$, the expected effect was large enough, so larger sample sizes were not necessary to demonstrate the magnitude of the effect. Data normalisation was performed on the thiamine uptake competition assay. Results are shown as the percentage of uptake compared to an unperturbed thiamine uptake experiment.

2.10 | Nomenclature of targets and ligands

Key protein targets and ligands in this article are hyperlinked to corresponding entries in http://www.guidetopharmacology.org, and are permanently archived in the Concise Guide to PHARMACOLOGY 2021/22 (Alexander, Christopoulos, Davenport, Kelly, Mathie, Peters, Veale, Armstrong, Faccenda, Harding, Davies, et al., 2023; Alexander, Cidlowski, Kelly, Mathie, Peters, Veale, Armstrong, Faccenda, Harding, Davies, Coons, et al., 2023; Alexander, Fabbro, Kelly, Mathie, Peters, Veale, Armstrong, Faccenda, Harding, Davies, & Amarosi, 2023; Alexander, Fabbro, Kelly, Mathie, Peters, Veale, Armstrong, Faccenda, Harding, Davies, Annett, et al., 2023; Alexander, Mathie, Peters, Veale, Striessnig, Kelly, Armstrong, Faccenda, Harding, Davies, Aldrich, et al., 2023).

3 | RESULTS

3.1 | Virtual screening using cryo-EM structures of SLC19A3

We recently determined the cryo-EM structures of SLC19A3 bound to its substrate thiamine and different known thiamine uptake inhibitors (TUIs, Gabriel et al., 2024). These structures not only revealed insights into the transport mechanisms and provided a detailed understanding how selected molecules interact with the transporter, but also indicated that the substrate binding site of SLC19A3 is rather promiscuous. To test this hypothesis, we used the available

experimental structures for a structure-based virtual screening (VS) campaign (Figure 1). To identify drugs that have the potential to inhibit SLC19A3, an ensemble docking approach was applied, in which 538 approved and investigational drugs were docked into the available SLC19A3 cryo-EM structures. Docking a virtual drug library into a set of structures complexed with different ligands allows to partly account for protein flexibility within the substrate binding site and was assumed to be a sensible approach for a transporter with a known broad ligand spectrum. The cryo-EM structures used here represent the inward-open state of SLC19A3 in the apo form (1), as well as substrate bound complexes withthiamine (2) and its known thiamine uptake inhibitors fedratinib (3), amprolium (4), **hydroxychloroquine** (5), and **amitriptyline** (6) (the numbers in parentheses indicate the ensemble structure numbers used in the following, see Table 1).

Initially, we assessed whether the molecular docking software GOLD can reproduce the ligand-binding mode of the five substances bound to the cryo-EM structures using ligand coordinates different from the ones present in the cryo-EM structures as input. The docking scores ranged from 59.6 (thiamine) to 90.6 (fedratinib) and the normalised scores (docking score divided by the number of non-hydrogen atoms) were mainly 3 or higher. The heavy atom root mean square deviation (RMSD) of the top-ranked docking poses indicated good reproducibility for amprolium (RMSD = 1.0 Å), hydroxychloroquine (1.2 Å), thiamine (2.0 Å), and amitriptyline (2.5 Å) (Table 1). Only the docking pose of fedratinib was in poor agreement with the experimentally determined binding mode (7.5 Å) (Table 1). Considering all 50 generated docking poses for fedratinib, the lowest RMSD was 7.1 Å. The overall re-docking performance confirmed GOLD as suitable for a VS campaign against SLC19A3. Subsequently, the small molecule library representing 538 different drugs (722 molecules including enantiomers), was docked into all six protein structures. In ensemble docking mode, GOLD provides information of the protein structure for which a given docking pose is obtained. Based on these data, for each of the six ensemble structures an individual hit list was generated that contained the compounds for which the top-ranked docking poses were obtained with this structure. About 50% of the top-ranked poses were assigned to the transporter structure obtained

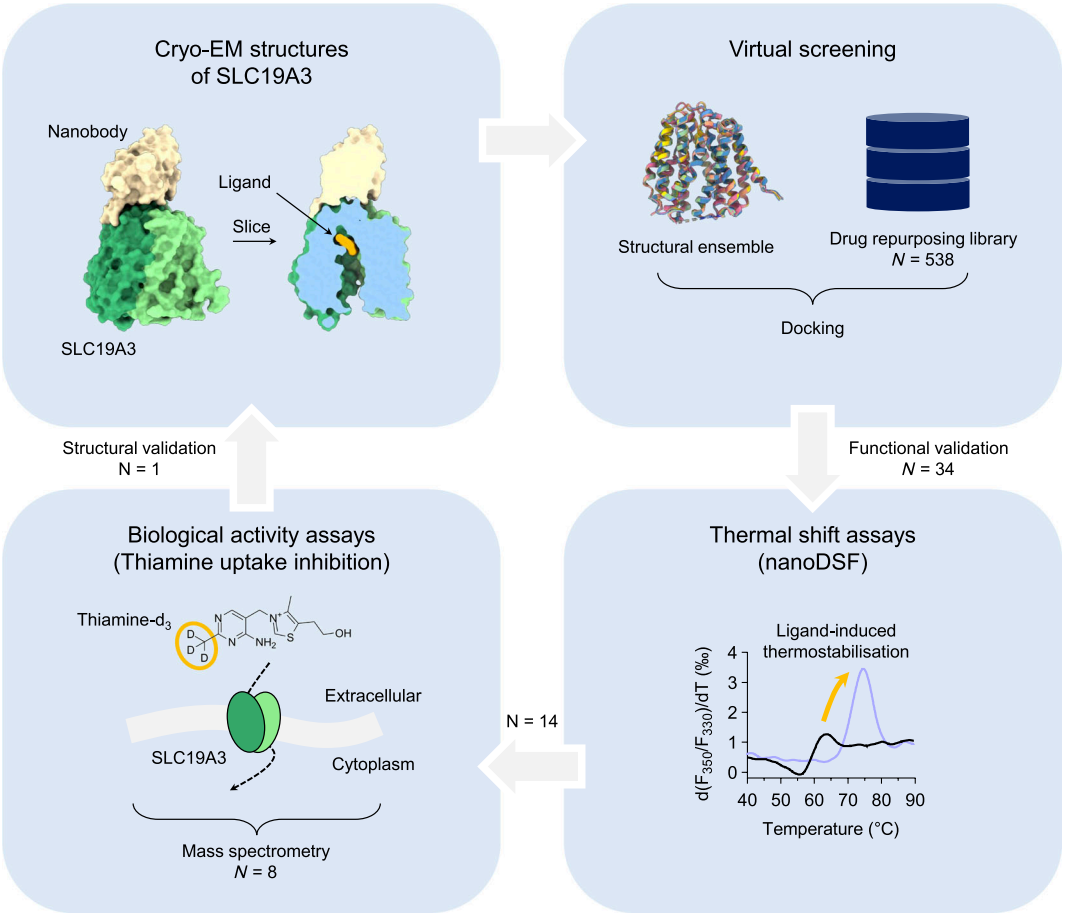

FIGURE 1 **Overview of the structure-based discovery process of inhibitors of the thiamine transporter SLC19A3.** Cryo-EM structures of the human SLC19A3 were previously determined using specific nanobodies as structural fiducials (Gabriel et al., 2024). These structures were used for virtual screening of a repurposing library comprising 538 drugs. 34 hit compounds of the virtual screening campaign were selected and experimentally tested for their interaction with SLC19A3 using a nanoDSF-based thermal shift assay. 14 compounds induced a thermostabilisation of SLC19A3. Eight novel compounds showed thiamine uptake inhibition in cellular assays. Cryo-EM was eventually used to experimentally investigate the binding mode of domperidone, one of the newly identified thiamine uptake inhibitors.

TABLE 1 Cryo-EM structures used for virtual screening.

Ligand in cryo-EM	PDB ID	Ensemble No.	RMSD[a]	Docking Score (normalised)[b]	Top-ranked docking poses[c]
Apo	9G5K	1	N/A	N/A	153
Thiamine	8S61	2	2.0 Å	59.6 (3.3)	106
Fedratinib	8S5W	3	7.5 Å	90.6 (2.4)	358
Amprolium	8S62	4	1.0 Å	60.4 (3.4)	30
Hydroxychloroquine	8S5Z	5	1.2 Å	69.6 (3.0)	16
Amitriptyline	n.dep.	6	2.5 Å	62.6 (3.0)	59

[a]Root mean square deviation (RMSD) between heavy atom positions of top-ranked docking pose and cryo-EM structure ligands.
[b]ChemPLP score for top-ranked docking pose and normalised score.
[c]Number of top-ranked docking poses assigned to the ensemble structure. n.dep.: not deposited. N/A: not applicable.

in complex with fedratinib (358), followed by the apo structure (153) and the thiamine-bound structure of SLC19A3 (106) (Table 1 & Supplementary Table S1). For a small number of compounds, the top-ranked poses were assigned to one of the other three ensemble structures (4: 30; 5: 16; 6: 59). We then visually inspected the protein-ligand interactions of each top-ranked docking pose and the corresponding transporter structure. Analysis of the VS results was done unaware of any SLC19A3 antagonists than the ones in the present cryo-EM structures. Altogether 34 compounds were selected for experimental validation based on the docking scores, the normalised docking scores, and visual inspection of the top-ranked 30% obtained for ensemble structures (1)–(3) and all compounds for structures (4)–(6) (Table 2).

3.2 | Experimental validation of SLC19A3 ligands

For the validation of the virtual hits, we tested the selected 34 compounds for their interaction with purified SLC19A3 using a thermal shift assay (nanoDSF). Five compounds, namely fluphenazine, naftopidil, sulfasalazine, famciclovir, and fluvastatin, interfered with the nanoDSF measurement at a compound concentration of 200 µM. We therefore repeated the measurements for these drugs at 20 µM. At this concentration, we could not observe any stabilising effect of these compounds on SLC19A3 (Supplementary Figure S1). Of the remaining 29 substances, 14 stabilized SLC19A3 *in vitro* (Figure 2a). The strongest effects ($\Delta T_m > +2\,^{\circ}C$, at 200 µM) were seen for **nefazodone**, domperidone, **chloroquine**, **trimethoprim**, and **etoricoxib**. Chloroquine and trimethoprim were already known to be TUIs (Giacomini et al., 2017). The fact that these compounds were picked up again by the docking procedure and the thermostabilisation screen validated our approach.

3.3 | Inhibitory potential of new SLC19A3 interactors in thiamine uptake assays

Compounds that stabilised SLC19A3 by more than 1 °C were selected to perform cell-based thiamine uptake inhibition assays. Initially, this assay was conducted with a low cell number (0.2×10^6 cells) and at a compound concentration of 20 µM (Figure 2b). Despite relatively large standard deviations (Figure 2b), these data indicated that nine out of the eleven tested SLC19A3 interactors interfere with thiamine uptake (Figure 2b). The strongest effects (> 40% inhibition) were induced by nefazodone, domperidone, **ketanserin**, and etoricoxib. Chloroquine was included as a positive control in this assay and completely suppressed thiamine uptake. To validate our findings, we repeated the cell-based uptake assay for nefazodone and domperidone under optimised conditions (Figure 2c). Compounds were purchased as dry stock material and the assay was carried out at a higher cell number and compound concentration (2×10^6 cells, 200 µM compound concentration). This confirmed the inhibition of SLC19A3-mediated thiamine uptake by nefazodone (36 ± 4%), domperidone (69 ± 2%), and the positive control fedratinib (91 ± 1%) (Figure 2c).

3.4 | Structural interaction profile of thiamine uptake inhibitors

To identify the relevant interactions of the binding and non-binding compounds, the top-ranked docking pose of each of the 34 selected molecules was analysed with respect to its molecular interactions with the corresponding SLC19A3 transporter structure of the ensemble (Figures 3 and 4). The same analysis was carried out for the five substances in the cryo-EM structures. None of the top-ranked docking poses of the identified transporter inhibitors revealed any polar interactions with seven amino acids in the binding site capable to form hydrogen bonds or salt bridges (Arg29, Glu32, Trp59, Thr117, Glu120, Thr324, and Tyr376). Hydrogen bonds between the inhibitors and SLC19A3 occur with Glu110 (six poses), Asn297 (three poses), Lys380 (two poses), and Glu320 (one pose). The hydrogen bonding pattern of the five inhibitors bound to the cryo-EM structures is similar. Three of those interact with Glu110 and only fedratinib forms a hydrogen bond with Glu32. Of the non-active compounds seven docking poses show an interaction with Glu32 and ten with Glu110.

We also investigated π-π stacking with Tyr113 and Tyr151. Of the ten inhibitors, nine exhibited stacking with Tyr113 and four with

TABLE 2 Overview of the docking results of the 34 selected hit compounds from the virtual screen.

Name	Score[a]	Structure[b]	# HA[c]	Norm. Score[d]	SlogP[e]	HBD[f]	TPSA[g]
Nefazodone	98.58	2	33	2.99	2.98	0	52.82
Fluvastatin (3*S*-5*R*)	94.41	6	30	3.15	3.39	2	85.52
Terfenadine (*R*)	94.26	2	35	2.69	5.44	2	44.9
Fluphenazine	91.15	3	30	3.04	3.2	1	31.15
Domperidone	88.23	2	30	2.94	3.18	2	69.12
Naftopidil (*R*)	86.94	3	29	3.00	1.99	1	46.37
Bepridil (*R*)	84.73	3	27	3.13	3.68	0	16.91
Alfuzosin (*S*)	84.65	3	28	3.02	0.77	1	113.08
Ketanserin	83.60	2	29	2.88	1.99	1	70.92
Bezafibrate	82.43	3	25	3.30	2.22	1	78.46
Chloroquine (*S*)	82.13	3	22	3.73	2.81	0	30.61
Loperamide	81.58	3	34	2.40	3.98	1	44.98
Buphenine (*RRS*)	81.10	2	22	3.69	2.49	2	57.07
Dobutamine (*S*)	79.50	3	22	3.61	1.93	3	77.3
Xamoterol (*R*)	76.76	5	24	3.20	−1.26	3	107.87
Celecoxib	74.35	6	26	2.86	3.83	1	77.98
Aztreonam	74.06	1	28	2.64	−2.85	2	201.25
Praziquantel (*R*)	72.24	6	23	3.14	2.63	0	40.62
Sulfasalazine	70.29	4	28	2.51	1.93	2	143.61
Etoricoxib	67.59	6	24	2.82	4.18	0	59.92
Famciclovir	67.14	4	23	2.92	0.81	1	122.22
Practolol (*S*)	65.71	6	19	3.46	0.36	2	75.17
Levallorphan	64.41	6	21	3.07	3.98	1	23.47
Fenbufen	63.18	6	19	3.33	2.07	0	57.2
Cimaterol (*R*)	60.16	6	16	3.76	0.24	2	86.65
Sotalol (*S*)	59.67	5	18	3.31	0.75	1	70.98
Trimethoprim	59.25	4	21	2.82	1.26	2	105.51
Oxibendazole	56.24	6	18	3.12	2.53	3	76.24
Zardaverine	55.89	6	19	2.94	2.9	0	67.3
Pantothenic-acid	53.87	4	15	3.59	−2.38	3	109.69
Moroxydine	51.93	5	12	4.33	−2.38	2	102.66
Phenylpropanolamine	50.31	4	11	4.57	0.45	1	47.87
Carbamylcholine	44.72	4	10	4.47	−0.21	1	52.32
4-amino-salicylic-acid	41.28	4	11	3.75	−0.66	2	86.38

[a]ChemPLP score.
[b]Ensemble protein structure for which docking pose with the highest score was obtained.
[c]Number of non-hydrogen atoms.
[d]ChemPLP score normalised to the number of non-hydrogen atoms.
[e–g]SlogP, number of hydrogen bond donor atoms (HBD), and topological polar surface area (TPSA).
The compounds highlighted in green stabilised SLC19A3 against heat denaturation and inhibited the transporter in cell-based thiamine uptake assays. (*R*) and (*S*) indicate the respective enantiomer. For the full list of the docking results, see Supplementary Table S1.

Tyr151. Interestingly, five of the docking poses stacking with Tyr113 formed a hydrogen bond with Glu110. All five compounds in the SLC19A3-inhibitor cryo-EM structures showed π-π stacking with Tyr113, while none of those interacted with Tyr151. Of the non-active compounds, half (12) demonstrated stacking with Tyr113 and two with Try151.

Based on the interaction studies a preliminary three-dimensional pharmacophore model was generated, composed of two aromatic features next to Tyr113 and Tyr151, two features for annotating the direction of the π-system of the aromatic features, as well as two hydrogen bond donor features reflecting the interactions with Glu110 and Asn297 (Figure 5). Screening the model with partial match (5 of

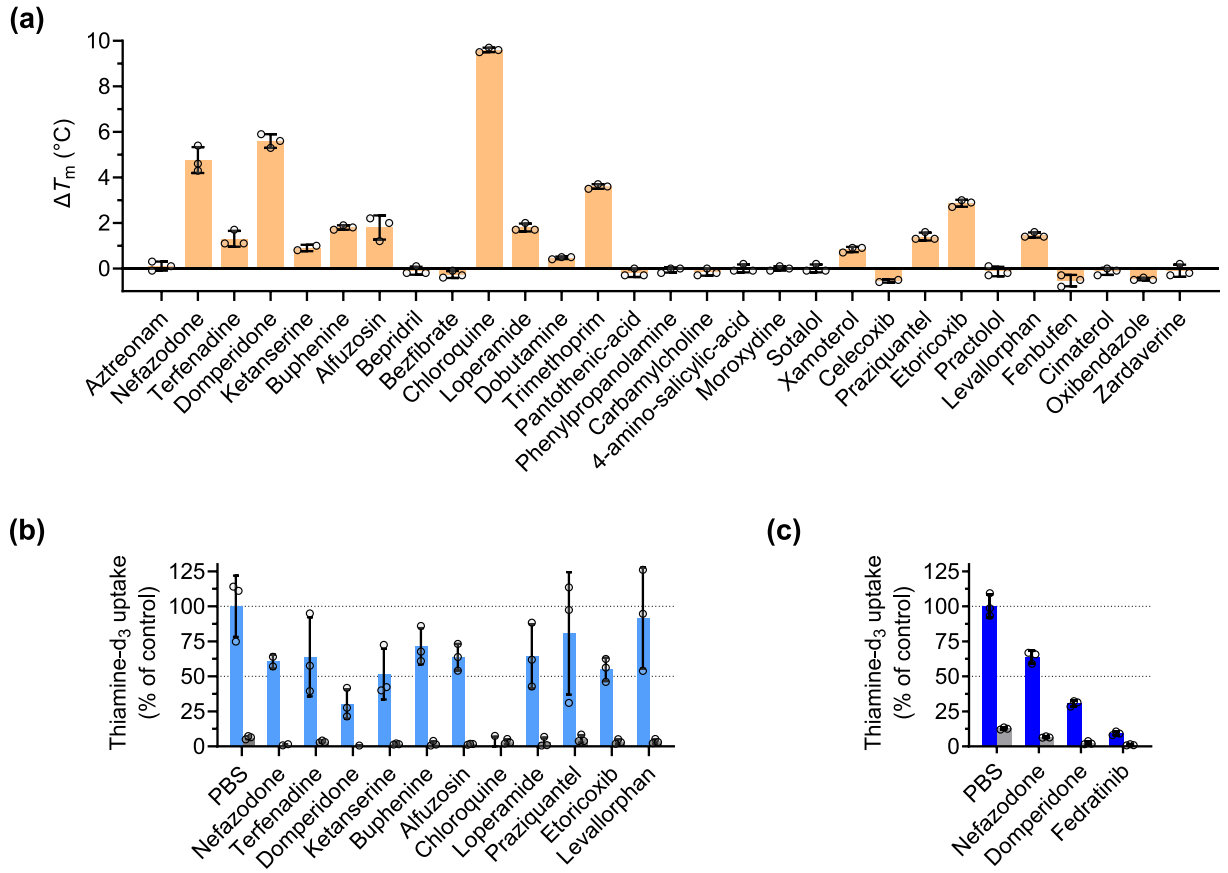

FIGURE 2 **Experimental validation of SLC19A3 virtual screening hits. (a)** Thermal shift assay (nanoDSF) of SLC19A3 in combination with 29 hit compounds from the structure-based virtual screen. SLC19A3 concentration: 4 μM. Compound concentration: 200 μM. **(b)** and **(c)** Mass spectrometry-based cellular thiamine-d_3 uptake assays. The bars show the thiamine-d_3 uptake by SLC19A3-transfected (blue) and mock transfected (grey) Expi293™ cells (mean ± s.d., $n = 3$, independent experiments). PBS: phosphate buffered saline (negative control). **(b)** Initial screen using 200,000 cells and 20 μM of the respective compounds. **(c)** Repetition of the assay for nefazodone, domperidone, and the positive control fedratinib with 2,000,000 cells and 200 μM compound concentration.

6 features needed to be fulfilled for a hit compound) using a conformation database of the 34 compounds (1595 conformations) resulted in seven compounds including four inhibitors (**terfenadine**, domperidone, ketanserin, **loperamide**). A pharmacophore search using a partial match of 4 resulted in 21 hits, including all inhibitors except etoricoxib.

3.5 | Cryo-EM structure of SLC19A3 in complex with domperidone

To experimentally validate the structural basis of the interaction of these newly identified inhibitors, we determined the cryo-EM structure of SLC19A3 in its inward-open state in complex with the confirmed TUI domperidone. Using thermal shift assays, we calculated an apparent binding affinity of domperidone for SLC19A3 in the low micromolar range ($K_{d,app}$ of 1.3 ± 0.2 μM) (Figure 6a). This affinity is comparable to the one determined for fedratinib (Gabriel et al., 2024). Cryo-EM samples were prepared by incubating SLC19A3 together with domperidone and the nanobody Nb3.3. EM data were collected and processed as summarised in Supplementary Figure S2 and described in detail in the methods section. The final reconstruction reached a global resolution of 3.35 Å. The structure of SLC19A3 and the nanobody could be modelled into the density map with high confidence (Supplementary Figure S3). The overall structure of SLC19A3 remained unchanged compared to the previously determined structures. The substrate binding site was well-resolved and clear density for a bound ligand (local resolution ≈ 2.8 Å) could be identified (Figure 6b). The molecular structure of domperidone matched the observed additional density (Figure 6c). The chloro-benzimidazole moiety of domperidone is inserting into the N-terminal domain (NTD) of SLC19A3 (Figure 6d). The chlorine atom is accommodated by the hydrophobic pocket created by Thr93, Trp94 and Leu97 on TM3, and Met106 and Val109 on TM4. As an aromatic ring system, the chloro-benzimidazole is engaging in π-π stacking with the aromatic clamp, mainly with Tyr113 and to a lesser extent with Phe56 and Trp59. The secondary ring amine of chloro-benzimidazole is in hydrogen bond distance to the side chain of Glu110 (3.1 Å). In addition, the carbonyl oxygen of the chloro-benzimidazole is in hydrogen bond distance with Asn297 (2.6 Å). The other major contact of domperidone with

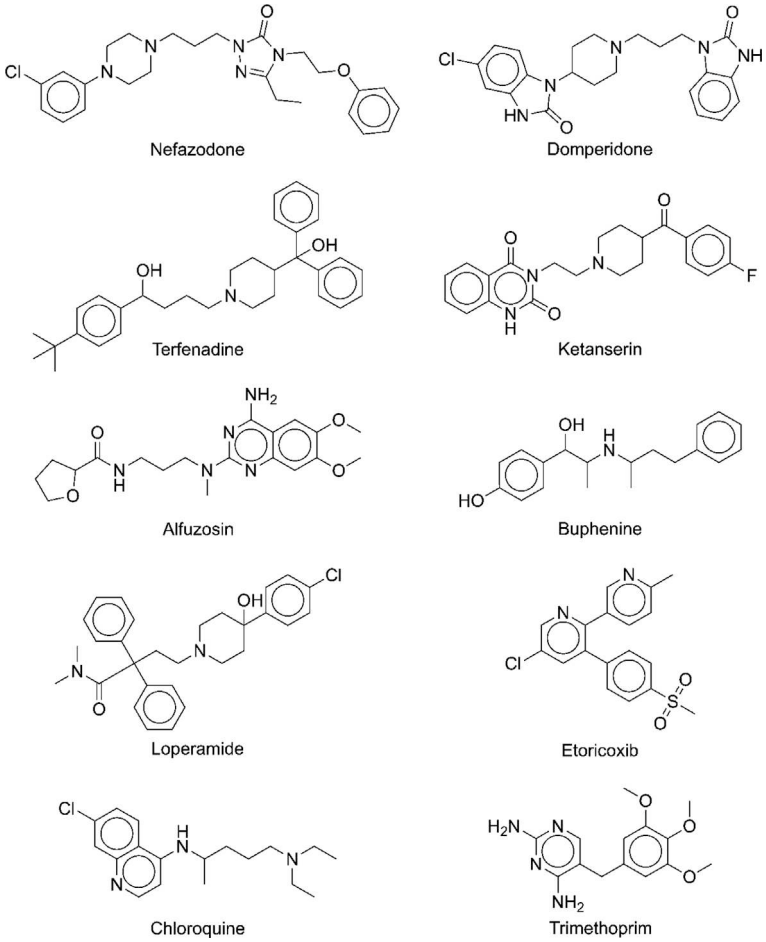

FIGURE 3 **Chemical structures of compounds inhibiting SLC19A3 mediated thiamine uptake.** Chloroquine and trimethoprim were already identified as thiamine uptake inhibitors (Vora et al., 2020). The remaining compounds showed inhibition of SLC19A3 in our cell-based uptake assays (Figure 2).

SLC19A3 is formed through its second aromatic moiety, the chlorine-free benzimidazole. The density for this part of the molecule is less well-defined. It can, however, be clearly located as an inserting moiety into a pocket between the transmembrane helices (TM) TM1b, TM5, and TM8. The benzimidazole is here primarily coordinated by a π-π stacking interaction with Tyr151 (Figure 6d). Overall, the domperidone molecule is wrapping around TM1b of the NTD of SLC19A3. The two benzimidazole groups of domperidone are anchored to the protein mainly by π-π stacking interactions. The linker connecting the two aromatic moieties provides the necessary flexibility for the drug molecule to fit in the substrate binding site of SLC19A3. Comparing the coordination of domperidone to other TUIs reveals interesting similarities and one important difference. The chloro-benzimidazole moiety of domperidone engages the transporter analogous to fedratinib, amprolium, and in particular hydroxychloroquine (Supplementary Figure S4). Its second benzimidazole moiety, however, forms an interaction network, which has not been observed for any other ligand of SLC19A3 so far (Figure 6d) (Dang et al., 2024; Gabriel et al., 2024; Li et al., 2024).

A comparison of the predicted binding mode for domperidone and the cryo-EM structure revealed a similar orientation of the compound within SLC19A3 (RMSD = 3.2 Å). The positioning of the chloro-benzimidazole moiety agrees well between the predicted and experimentally determined structures. The other benzimidazole of domperidone is engaging Tyr151 in an unpredicted manner. While the docking pose locates this moiety in the central vestibule of SLC19A3, the cryo-EM structure illustrates that this part inserts into a pocket on the other side of Tyr151 (Figure 6d).

4 | DISCUSSION

Virtual screening is a frequently used approach to identify putative bioactive compounds within large compound libraries (da Silva Rocha et al., 2019; Sabe et al., 2021). Molecular docking is probably the most popular technique for structure-based virtual screening. It makes use of experimentally obtained structures, mainly by X-ray crystallography, or structures resulting from prediction methods such as AlphaFold or conventional protein modelling approaches such as SWISS-MODEL (Abramson et al., 2024; Waterhouse et al., 2018). Despite the increasing number of cryo-EM structures in public databases, only a limited number of studies using these structures for virtual screening have been published (Hughes et al., 2019; Xia et al., 2023; Yu et al., 2024). Small molecule docking programs usually do not consider protein flexibility. To account for the local structural flexibility of the transporter, an ensemble docking approach was chosen here, in which

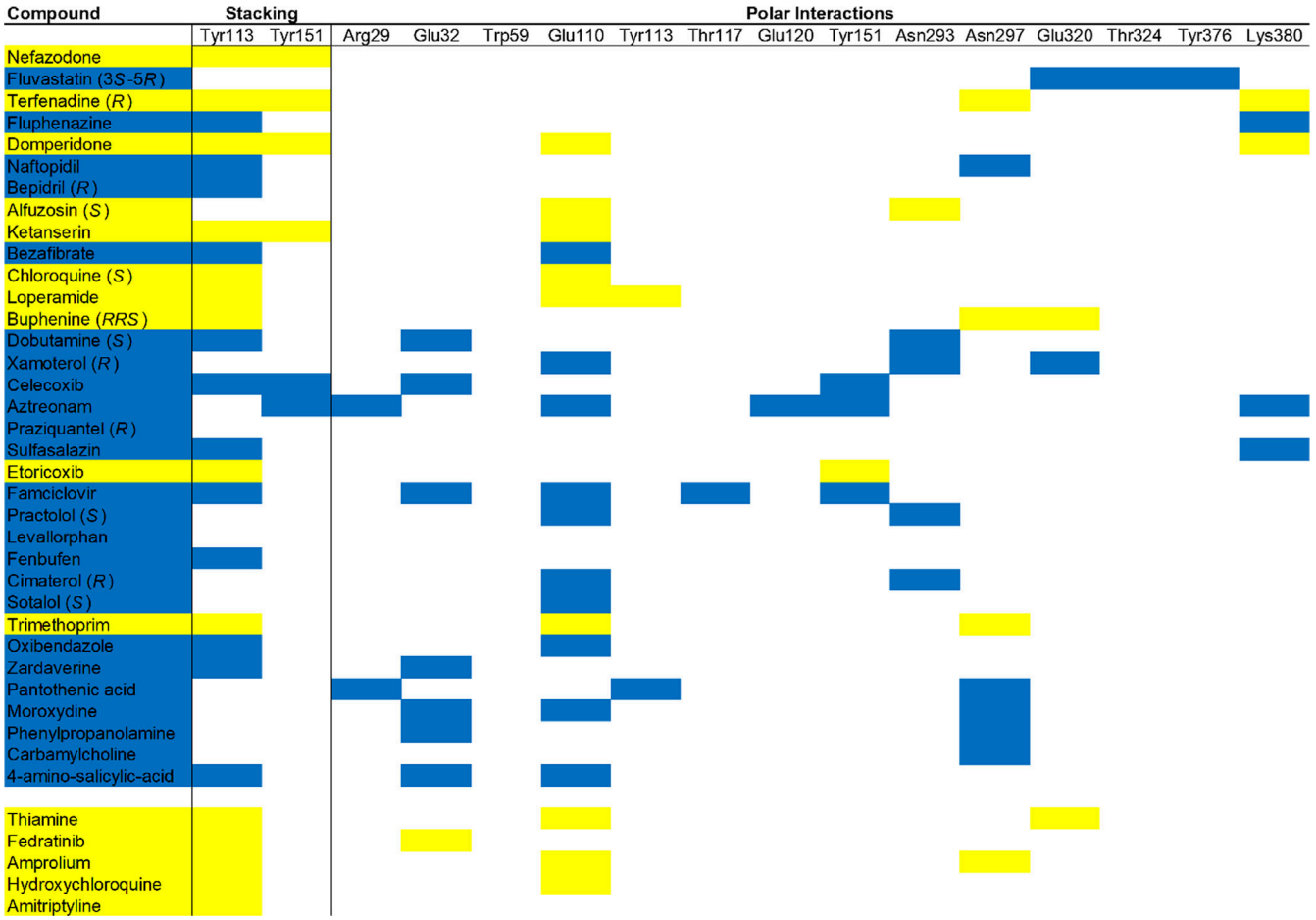

FIGURE 4 **Protein-ligand interactions with SLC19A3.** Coloured boxes indicate an interaction of a compound with the respective amino acid residue of SLC19A3. Yellow: Experimentally confirmed interaction of the compound with SLC19A3 and thiamine uptake inhibition. Blue: No interaction between the compound and SLC19A3 *in vitro*.

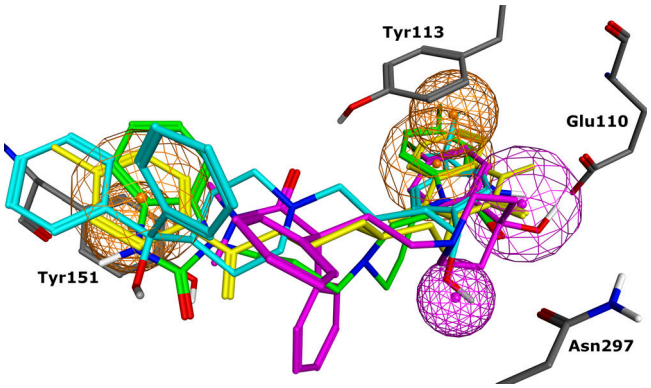

FIGURE 5 **Pharmacophore model for SLC19A3 inhibitors.** Large orange spheres indicate aromatic features, small orange spheres annotate the direction of the π-system of the aromatic feature, while pink spheres annotate two hydrogen bond donors. Top-ranked docking poses of domperidone (carbon atoms in green), terfenadine (cyan), ketanserin (yellow), and loperamide (pink) as well as four amino acids of SLC19A3 are shown in capped sticks.

the small molecule library was docked into six cryo-EM structures superposed on each other. Docking scores provide a general guideline for selecting compounds for experimental validation, but rarely correlate well with experimental data. Thus, virtual screening is, in contrast to experimental screening approaches, associated with a high number of false-positive hits. Based on visual analysis of top-ranked poses for nefazodone, terfenadine, domperidone, ketanserin and buphenine docked into structure (2), the compounds were selected for experimental testing and all of them proved to be SLC19A3 inhibitors. Three of these were among the 10 top-ranked small molecules for this protein. Three of the eight selected compounds for which the top-ranked docking poses were assigned to structure (3) inhibited SLC19A3. For structure (4) and the amitriptyline-bound structure (6), one of the selected compounds demonstrated transporter inhibition, while none of the compounds selected based on their docking score obtained with structure (1) or (5) inhibited SLC19A3.

Recent studies (Gabriel et al., 2024; Li et al., 2024; Vora et al., 2020) and the findings of this present work indicate that SLC19A3 is a relatively promiscuous transporter with respect to drug

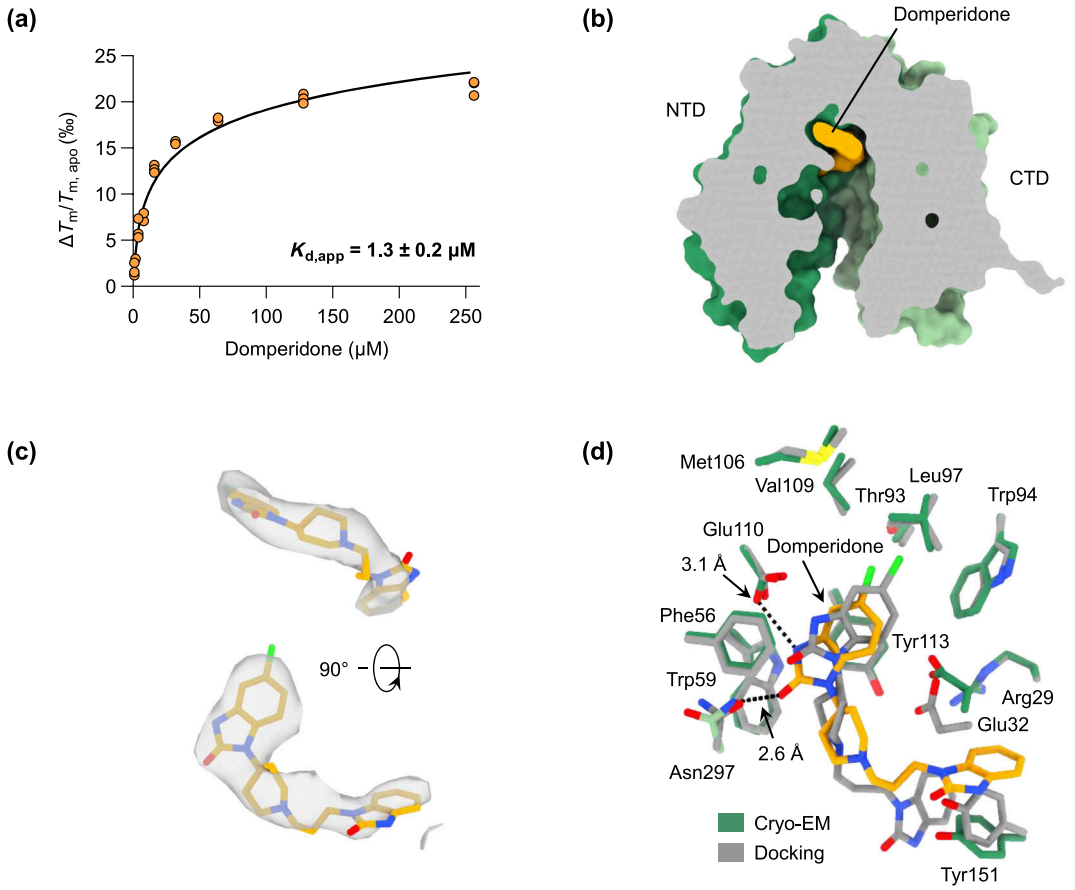

FIGURE 6 **Cryo-EM structure of domperidone-bound SLC19A3. (a)** Thermal shift assay (nanoDSF) for the determination of the apparent binding affinity of domperidone to SLC19A3-wt ($n = 3$, technical replicates). **(b)** Slice through a surface representation of the SLC19A3-domperidone complex. The NTD and CTD of the transporter are coloured in dark and light green, respectively. Domperidone is highlighted in orange. **(c)** Cryo-EM density (grey surface) and modelled domperidone structure (map contour level: 0.65). **(d)** Substrate binding site of SLC19A3. Comparison of the domperidone binding pose between the experimental cryo-EM structure (side chains are shown in green and domperidone in orange) and the top-ranked docking pose in structure (2) (side chains and domperidone are shown in grey). The docking approach predicted the localisation of the chloro-benzimidazole moiety largely correctly. The second benzimidazole, however, engages the transporter in an unpredicted manner, by inserting into a pocket behind Tyr151.

binding. This phenomenon is already known for the well-studied **SLC15 family** (Killer et al., 2021; Kotov et al., 2023; Parker et al., 2024), the lysosomal peptide transporter MFSD1 (Jungnickel et al., 2024) and the human ether-a-go-go-related gene **(hERG) K^+ channel**. The blockage of hERG by drugs can result in the so-called drug-induced long QT syndrome and an increased risk of sudden death. Several drugs have been withdrawn due to their cardiotoxic side effects or sold with cautionary labels (Kalyaanamoorthy & Barakat, 2018). Moreover, the xenobiotic sensor **pregnane X receptor**, a ligand-modulated transcription factor responsible for detecting potentially harmful compounds, is also known to be activated by a structurally diverse set of compounds, including many approved drugs (Lv et al., 2022).

Of the approved drugs already identified as inhibitors of SLC19A3 (Liang et al., 2015; Vora et al., 2020), a few were present in our screening library. The **angiotensin converting enzyme** inhibitor **quinapril** ($IC_{50} = 34$ µM) ranked 29th on the hit list obtained for structure (2). The screened database also included the antibiotic trimethoprim ($IC_{50} = 5.6$ µM). The compound was on rank 7 considering the hit list for structure (4). The tricyclic antidepressant amitriptyline ($IC_{50} = 11.3$ µM) ranked 170th on the hit list for structure (3). Despite the fact that structure (6) was obtained in complex with this compound, the docking score of the re-docking study (62.6) was lower compared to the score when docked into structure (3) (68.8). The (*R*)-enantiomer of the calcium channel blocker **verapamil** ($IC_{50} = 141$ µM) ranked 13th on the hit list for structure (1), while the (*S*)-enantiomer ranked 42nd for structure (3). Very recently, a cryo-EM structure of SLC19A3 in complex with the SLC19A3 inhibitor **metformin** (PDB ID: 8Z7W), an antidiabetic drug, has been published (Li et al., 2024). This compound was also present in the screened library and ranked 19th on the hit list for structure (4). The docking score of 42.7 obtained with structure (4) is low (Supplementary Table S1), however the normalised score (4.74) is above the normalised score for any of the 34 compounds selected for experimental testing, emphasising the relevance of this criterion for analysing virtual screening data. The predicted binding mode of metformin is

similar to the position in the cryo-EM structure (RMSD = 1.7 Å). These results imply that the hit list is likely to contain additional SLC19A3 inhibitors among the top-ranked compounds (score and normalised score).

Our workflow of virtual screening coupled with the experimental validation pipeline significantly expands the list of known SLC19A3 inhibitors. Further studies are needed to identify additional compounds interfering with this transporter. Molecular docking appears to be a useful approach for the rapid assessment of transporter binding. So far, analysis of bioactivity data of inhibitors and non-inhibitors had revealed that SLC19A3 inhibitors tend to be more lipophilic due to higher SLogP and a lower number of hydrogen bond donors and acceptors as well as a lower total polar surface area (Vora et al., 2020). This is confirmed by our study. The average SlogP of SLC19A3 inhibitors is higher than that of non-inhibitors (2.91 vs. 1.33), while the number of hydrogen bond donors (1.10 vs. 1.44) and the topological surface area (64.9 vs. 76.3) is lower. Only three TUIs (**alfuzosin**, trimethoprim, ketanserin) feature a SlogP below 2. In contrast, the SlogP of ten non-active compounds is above 2.

According to the docking data analysis, π-π stacking with Tyr113 is important for ligand binding. In contrast, binding modes resulting in hydrogen bond formation with Glu32 appear to be associated with a lower likelihood of transporter binding. Based on the interaction data for the 34 compounds it is possible to develop a rule-based model for prioritising docked compounds emerging from a virtual screen to be tested experimentally. Considering only compounds showing stacking with Tyr113, no hydrogen bond formation with Glu32 and a hydrogen bond shared with either Glu110 or Asn297 would result in a set of 11 substances to be tested, of which only three (naftopidil, bezafibrate, oxibendazole) did not inhibit the transporter. However, based on these criteria, only three of the five compounds bound to the cryo-EM structures would be selected (thiamine, amprolium, hydroxychloroquine). Pharmacophore models allow investigators to assess whether structurally different molecules can bind to a target via interactions considered as relevant for the pharmacological effect (Giordano et al., 2022). Our model incorporates only few features that appear to be relevant for transporter inhibition. Due to the limited resolution of the cryo-EM structures, as well as predicted binding modes used for selecting the features, the accuracy of the model is limited. Compounds without any hydrogen bond donors, such as etoricoxib, cannot be identified with the model as it includes only aromatic and hydrogen bond donor features. Future efforts may include further structural and quantitative data such as binding studies, to develop a more accurate model for predicting SLC19A3 inhibition.

The findings presented in this study on SLC19A3 represent a significant advance in the elucidation of the drug interactions of this essential transporter. Future research should evaluate thiamine uptake inhibitors (TUIs) identified through in silico and in vitro analyses for their effects on thiamine transport and metabolism in humans, particularly in individuals predisposed to thiamine deficiencies due to pre-existing conditions. In healthy individuals, compensatory mechanisms are likely to mitigate the temporary inhibition of thiamine transporters. These mechanisms may include alternative transport pathways for thiamine and thiamine pyrophosphate (thiamine-pp) via other membrane transporters, such as **OCT1/2** and **SLC44A4** (Anandam et al., 2017; Chen et al., 2014; Nabokina et al., 2014). Additionally, human cells possess a limited storage capacity for vitamin B_1, which may provide short-term resilience against impaired thiamine uptake (Mrowicka et al., 2023).

However, drug interactions affecting thiamine transporters may have more severe consequences in populations at risk for thiamine deficiencies. These vulnerable groups include individuals with one or more of the following risk factors: (i) malnutrition (e.g., due to limited food supply, anorexia nervosa, or chemotherapy); (ii) inflammatory bowel diseases such as Crohn's disease; (iii) chronic alcohol consumption; (iv) concurrent treatment with other TUIs (e.g., fedratinib, tricyclic antidepressants); and (v) genetic defects in thiamine transport and metabolism, including heterozygous carriers of pathogenic variants of *SLC19A2*, *SLC19A3*, *TPK1*, and ***SLC25A19***.

Collectively, these risk factors may predispose a substantial number of individuals to drug-induced thiamine deficiencies. Therefore, careful monitoring and adequate thiamine supplementation should be prioritised in these patient populations. Moreover, the concept of drug-induced inhibition of essential vitamin transporters may extend beyond thiamine to other key micronutrients. This includes the riboflavin (vitamin B_2) transporters (SLC52A1–3), the folate (vitamin B_9) transporters (SLC19A1 and SLC46A1), and the ascorbic acid (vitamin C) transporters (SLC23A1–3). Accordingly, we propose a broader framework of vitamin uptake inhibition (VUI) that should be systematically evaluated in drug safety assessments. Conversely, vitamin transporters may also serve as potential targets for drug delivery. Many vitamin transporters exist in groups of functionally very similar proteins (e.g. SLC19A2 and SLC19A3) with distinct tissue- and cell-specific expression patterns. A deeper understanding of their structural differences could enable their exploitation as selective drug transport routes within the human body.

AUTHOR CONTRIBUTIONS

Florian Gabriel: Conceptualization; investigation; visualization; writing. **Björn Windshügel:** Conceptualization; investigation; visualization; project administration; writing. **Christian Löw:** Conceptualization; project administration; funding acquisition; writing. All authors have read and agreed to the published version of the manuscript.

ACKNOWLEDGMENTS

We thank the Sample Preparation and Characterisation facility at EMBL (Hamburg, Germany) and the team of the cryo-EM Facility at CSSB for their support, technical assistance and advice. We want to acknowledge all group members for fruitful discussions and continuous support and feedback on the project. Part of this work was performed at the CryoEM Facility at CSSB, supported by the UHH and DFG (grant numbers INST 152/772-1|152/774-1|152/775-1|152/776-1|152/777-1 FUGG).

CONFLICT OF INTEREST STATEMENT

The authors declare no conflicting interests.

DATA AVAILABILITY STATEMENT

The EM data and fitted model for hSLC19A3 bound to domperidone have been deposited in the Electron Microscopy Data Bank and the PDB under the following accession codes: hSLC19A3-wt: Nb3.3-domperidone (PDB ID: 9HJD, EMD-52213).

DECLARATION OF TRANSPARENCY AND SCIENTIFIC RIGOUR

This Declaration acknowledges that this paper adheres to the principles for transparent reporting and scientific rigour of preclinical research as stated in the BJP guidelines for Design and Analysis, and as recommended by funding agencies, publishers and other organisations engaged with supporting research.

MATERIALS AVAILABILITY

All reagents generated in this study are available from the corresponding authors upon reasonable request.

ORCID

Florian Gabriel https://orcid.org/0000-0002-2528-6506
Björn Windshügel https://orcid.org/0000-0002-4835-3134
Christian Löw https://orcid.org/0000-0003-0764-7483

REFERENCES

Abramson, J., Adler, J., Dunger, J., Evans, R., Green, T., Pritzel, A., Ronneberger, O., Willmore, L., Ballard, A. J., Bambrick, J., Bodenstein, S. W., Evans, D. A., Hung, C. C., O'Neill, M., Reiman, D., Tunyasuvunakool, K., Wu, Z., Žemgulytė, A., Arvaniti, E., … Jumper, J. M. (2024). Accurate structure prediction of biomolecular interactions with AlphaFold 3. *Nature*, *630*, 493–500. https://doi.org/10.1038/s41586-024-07487-w

Afonine, P. V., Poon, B. K., Read, R. J., Sobolev, O. V., Terwilliger, T. C., Urzhumtsev, A., & Adams, P. D. (2018). Real-space refinement in PHENIX for cryo-EM and crystallography. *Acta Crystallographica Section D, Structural Biology*, *74*, 531–544. https://doi.org/10.1107/S2059798318006551

Alexander, S. P. H., Christopoulos, A., Davenport, A. P., Kelly, E., Mathie, A. A., Peters, J. A., Veale, E. L., Armstrong, J. F., Faccenda, E., Harding, S. D., Davies, J. A., Abbracchio, M. P., Abraham, G., Agoulnik, A., Alexander, W., Al-Hosaini, K., Bäck, M., Baker, J. G., Barnes, N. M., … Ye, R. D. (2023). The Concise Guide to PHARMACOLOGY 2023/24: G protein-coupled receptors. *British Journal of Pharmacology*, *180*(Suppl 2), S23–S144. https://doi.org/10.1111/bph.16177

Alexander, S. P. H., Cidlowski, J. A., Kelly, E., Mathie, A. A., Peters, J. A., Veale, E. L., Armstrong, J. F., Faccenda, E., Harding, S. D., Davies, J. A., Coons, L., Fuller, P. J., Korach, K. S., & Young, M. J. (2023). The Concise Guide to PHARMACOLOGY 2023/24: Nuclear hormone receptors. *British Journal of Pharmacology*, *180*(Suppl 2), S223–S240. https://doi.org/10.1111/bph.16179

Alexander, S. P. H., Fabbro, D., Kelly, E., Mathie, A. A., Peters, J. A., Veale, E. L., Armstrong, J. F., Faccenda, E., Harding, S. D., Davies, J. A., & Amarosi, L. (2023). The Concise gGide to PHARMACOLOGY 2023/24: Transporters. *British Journal of Pharmacology*, *180*(Suppl 2), S374–S469.

Alexander, S. P. H., Fabbro, D., Kelly, E., Mathie, A. A., Peters, J. A., Veale, E. L., Armstrong, J. F., Faccenda, E., Harding, S. D., Davies, J. A., Annett, S., Boison, D., Burns, K. E., Dessauer, C., Gertsch, J., Helsby, N. A., Izzo, A. A., Ostrom, R., Papapetropoulos, A., … Wong, S. S. (2023). The Concise Guide to PHARMACOLOGY 2023/24: Enzymes. *British Journal of Pharmacology*, *180*(Suppl 2), S289–S373. https://doi.org/10.1111/bph.16181

Alexander, S. P. H., Mathie, A. A., Peters, J. A., Veale, E. L., Striessnig, J., Kelly, E., Armstrong, J. F., Faccenda, E., Harding, S. D., Davies, J. A., Aldrich, R. W., Attali, B., Baggetta, A. M., Becirovic, E., Biel, M., Bill, R. M., Caceres, A. I., Catterall, W. A., Conner, A. C., … Zhu, M. (2023). The Concise Guide to PHARMACOLOGY 2023/24: Ion channels. *British Journal of Pharmacology*, *180*(Suppl 2), S145–S222. https://doi.org/10.1111/bph.16178

Alfadhel, M., Umair, M., Almuzzaini, B., Alsaif, S., AlMohaimeed, S. A., Almashary, M. A., Alharbi, W., Alayyar, L., Alasiri, A., Ballow, M., AlAbdulrahman, A., Alaujan, M., Nashabat, M., Al-Odaib, A., Altwaijri, W., Al-Rumayyan, A., Alrifai, M. T., Alfares, A., AlBalwi, M., & Tabarki, B. (2019). Targeted *SLC19A3* gene sequencing of 3000 Saudi newborn: A pilot study toward newborn screening. *Annals of Clinical and Translational Neurology*, *6*, 2097–2103. https://doi.org/10.1002/acn3.50898

Anandam, K. Y., Srinivasan, P., Subramanian, V. S., & Said, H. M. (2017). Molecular mechanisms involved in the adaptive regulation of the colonic thiamin pyrophosphate uptake process. *American Journal of Physiology-Cell Physiology*, *313*, C655–C663.

Baker, L. J., Dorocke, J. A., Harris, R. A., & Timm, D. E. (2001). The crystal structure of yeast thiamin pyrophosphokinase. *Structure*, *9*, 539–546. https://doi.org/10.1016/S0969-2126(01)00615-3

Chen, L., Shu, Y., Liang, X., Chen, E. C., Yee, S. W., Zur, A. A., Li, S., Xu, L., Keshari, K. R., Lin, M. J., Chien, H. C., Zhang, Y., Morrissey, K. M., Liu, J., Ostrem, J., Younger, N. S., Kurhanewicz, J., Shokat, K. M., Ashrafi, K., & Giacomini, K. M. (2014). OCT1 is a high-capacity thiamine transporter that regulates hepatic steatosis and is a target of metformin. *Proceedings of the National Academy of Sciences of the United States of America*, *111*(27), 9983–9988. https://doi.org/10.1073/pnas.1314939111

Croll, T. I. (2018). ISOLDE: A physically realistic environment for model building into low-resolution electron-density maps. *Acta Crystallographica Section D, Structural Biology*, *74*, 519–530. https://doi.org/10.1107/S2059798318002425

Curtis, M. J., Alexander, S. P. H., Cirino, G., George, C. H., Kendall, D. A., Insel, P. A., Izzo, A. A., Ji, Y., Panettieri, R. A., Patel, H. H., Sobey, C. G., Stanford, S. C., Stanley, P., Stefanska, B., Stephens, G. J., Teixeira, M. M., Vergnolle, N., & Ahluwalia, A. (2022). Planning experiments: Updated guidance on experimental design and analysis and their reporting III. *British Journal of Pharmacology*, *179*, 3907–3913. https://doi.org/10.1111/bph.15868

da Silva Rocha, S. F. L., Olanda, C. G., Fokoue, H. H., & Sant'Anna, C. M. R. (2019). Virtual screening techniques in drug discovery: Review and recent applications. *Current Topics in Medicinal Chemistry*, *19*, 1751–1767. https://doi.org/10.2174/1568026619666190816101948

Dang, Y., Zhang, T., Pidathala, S., Wang, G., Wang, Y., Chen, N., Song, C., Lee, C. H., & Zhang, Z. (2024). Substrate and drug recognition mechanisms of SLC19A3. *Cell Research*, *34*, 458–461. https://doi.org/10.1038/s41422-024-00951-2

Drew, D., North, R. A., Nagarathinam, K., & Tanabe, M. (2021). Structures and general transport mechanisms by the major facilitator superfamily (MFS). *Chemical Reviews*, *121*, 5289–5335. https://doi.org/10.1021/acs.chemrev.0c00983

Dutta, B., Huang, W., Molero, M., Kekuda, R., Leibach, F. H., Devoe, L. D., Ganapathy, V., & Prasad, P. D. (1999). Cloning of the human thiamine transporter, a member of the folate transporter family. *Journal of Biological Chemistry*, *274*, 31925–31929. https://doi.org/10.1074/jbc.274.45.31925

Emsley, P., Lohkamp, B., Scott, W. G., & Cowtan, K. (2010). Features and development of coot. *Acta Crystallogr D Biol Crystallogr*, *66*, 486–501. https://doi.org/10.1107/S0907444910007493

Gabriel, F., Spriestersbach, L., Fuhrmann, A., Jungnickel, K. E. J., Mostafavi, S., Pardon, E., Steyaert, J., & Löw, C. (2024). Structural basis of thiamine transport and drug recognition by SLC19A3. *Nature Communications*, *15*, 8542. https://doi.org/10.1038/s41467-024-52872-8

Giacomini, M. M., Hao, J., Liang, X., Chandrasekhar, J., Twelves, J., Whitney, J. A., Lepist, E. I., & Ray, A. S. (2017). Interaction of 2,4-Diaminopyrimidine-containing drugs including Fedratinib and trimethoprim with thiamine transporters. *Drug Metabolism and Disposition*, *45*, 76–85. https://doi.org/10.1124/dmd.116.073338

Giordano, D., Biancaniello, C., Argenio, M. A., & Facchiano, A. (2022). Drug design by pharmacophore and virtual screening approach. *Pharmaceuticals (Basel)*, *15*, 646. https://doi.org/10.3390/ph15050646

Hall, J. (2019). A simple model for determining affinity from irreversible thermal shifts. *Protein Science*, *28*, 1880–1887. https://doi.org/10.1002/pro.3701

Hughes, T. E., Del Rosario, J. S., Kapoor, A., Yazici, A. T., Yudin, Y., Fluck, E. C. 3rd, Filizola, M., Rohacs, T., & Moiseenkova-Bell, V. Y. (2019). Structure-based characterization of novel TRPV5 inhibitors. *eLife*, *8*, e49572. https://doi.org/10.7554/eLife.49572

Jardetzky, O. (1966). Simple allosteric model for membrane pumps. *Nature*, *211*, 969–970. https://doi.org/10.1038/211969a0

Jumper, J., Evans, R., Pritzel, A., Green, T., Figurnov, M., Ronneberger, O., Tunyasuvunakool, K., Bates, R., Žídek, A., Potapenko, A., Bridgland, A., Meyer, C., Kohl, S. A. A., Ballard, A. J., Cowie, A., Romera-Paredes, B., Nikolov, S., Jain, R., Adler, J., … Hassabis, D. (2021). Highly accurate protein structure prediction with AlphaFold. *Nature*, *596*, 583–589. https://doi.org/10.1038/s41586-021-03819-2

Jungnickel, K. E. J., Guelle, O., Iguchi, M., Dong, W., Kotov, V., Gabriel, F., Debacker, C., Dairou, J., McCort-Tranchepain, I., Laqtom, N. N., Chan, S. H., Ejima, A., Sato, K., Massa López, D., Saftig, P., Mehdipour, A. R., Abu-Remaileh, M., Gasnier, B., Löw, C., & Damme, M. (2024). MFSD1 with its accessory subunit GLMP functions as a general dipeptide uniporter in lysosomes. *Nature Cell Biology*, *26*, 1047–1061. https://doi.org/10.1038/s41556-024-01436-5

Kalyaanamoorthy, S., & Barakat, K. H. (2018). Development of safe drugs: The hERG challenge. *Medicinal Research Reviews*, *38*, 525–555. https://doi.org/10.1002/med.21445

Killer, M., Wald, J., Pieprzyk, J., Marlovits, T. C., & Low, C. (2021). Structural snapshots of human PepT1 and PepT2 reveal mechanistic insights into substrate and drug transport across epithelial membranes. *Science Advances*, *7*, eabk3259. https://doi.org/10.1126/sciadv.abk3259

Kono, S., Miyajima, H., Yoshida, K., Togawa, A., Shirakawa, K., & Suzuki, H. (2009). Mutations in a thiamine-transporter gene and Wernicke's-like encephalopathy. *New England Journal of Medicine*, *360*, 1792–1794. https://doi.org/10.1056/NEJMc0809100

Kotov, V., Killer, M., Jungnickel, K. E. J., Lei, J., Finocchio, G., Steinke, J., Bartels, K., Strauss, J., Dupeux, F., Humm, A. S., Cornaciu, I., Márquez, J. A., Pardon, E., Steyaert, J., & Löw, C. (2023). Plasticity of the binding pocket in peptide transporters underpins promiscuous substrate recognition. *Cell Reports*, *42*, 112831. https://doi.org/10.1016/j.celrep.2023.112831

Li, P., Zhu, Z., Wang, Y., Zhang, X., Yang, C., Zhu, Y., Zhou, Z., Chao, Y., Long, Y., Gao, Y., Liu, S., Zhang, L., Gao, P., & Qu, Q. (2024). Substrate transport and drug interaction of human thiamine transporters SLC19A2/A3. *Nature Communications*, *15*, 10924. https://doi.org/10.1038/s41467-024-55359-8

Liang, X., Chien, H. C., Yee, S. W., Giacomini, M. M., Chen, E. C., Piao, M., Hao, J., Twelves, J., Lepist, E. I., Ray, A. S., & Giacomini, K. M. (2015). Metformin is a substrate and inhibitor of the human thiamine transporter, THTR-2 (SLC19A3). *Molecular Pharmaceutics*, *12*, 4301–4310. https://doi.org/10.1021/acs.molpharmaceut.5b00501

Lv, Y., Luo, Y. Y., Ren, H. W., Li, C. J., Xiang, Z. X., & Luan, Z. L. (2022). The role of pregnane X receptor (PXR) in substance metabolism. *Frontiers in Endocrinology (Lausanne)*, *13*, 959902. https://doi.org/10.3389/fendo.2022.959902

Manzetti, S., Zhang, J., & van der Spoel, D. (2014). Thiamin function, metabolism, uptake, and transport. *Biochemistry*, *53*, 821–835. https://doi.org/10.1021/bi401618y

Mrowicka, M., Mrowicki, J., Dragan, G., & Majsterek, I. (2023). The importance of thiamine (vitamin B1) in humans. *Bioscience Reports*, *43*(10), BSR20230374. https://doi.org/10.1042/BSR20230374

Nabokina, S. M., Inoue, K., Subramanian, V. S., Valle, J. E., Yuasa, H., & Said, H. M. (2014). Molecular identification and functional characterization of the human colonic thiamine pyrophosphate transporter. *The Journal of Biological Chemistry*, *289*(7), 4405–4416. https://doi.org/10.1074/jbc.M113.528257

Pardanani, A., Harrison, C., Cortes, J. E., Cervantes, F., Mesa, R. A., Milligan, D., Masszi, T., Mishchenko, E., Jourdan, E., Vannucchi, A. M., Drummond, M. W., Jurgutis, M., Kuliczkowski, K., Gheorghita, E., Passamonti, F., Neumann, F., Patki, A., Gao, G., & Tefferi, A. (2015). Safety and efficacy of fedratinib in patients with primary or secondary myelofibrosis: A randomized clinical trial. *JAMA Oncology*, *1*, 643–651. https://doi.org/10.1001/jamaoncol.2015.1590

Parker, J. L., Deme, J. C., Lichtinger, S. M., Kuteyi, G., Biggin, P. C., Lea, S. M., & Newstead, S. (2024). Structural basis for antibiotic transport and inhibition in PepT2. *Nature Communications*, *15*, 8755. https://doi.org/10.1038/s41467-024-53096-6

Pettersen, E. F., Goddard, T. D., Huang, C. C., Meng, E. C., Couch, G. S., Croll, T. I., Morris, J. H., & Ferrin, T. E. (2021). UCSF ChimeraX: Structure visualization for researchers, educators, and developers. *Protein Science*, *30*, 70–82. https://doi.org/10.1002/pro.3943

Pintilie, G., Zhang, K., Su, Z., Li, S., Schmid, M. F., & Chiu, W. (2020). Measurement of atom resolvability in cryo-EM maps with Q-scores. *Nature Methods*, *17*, 328–334. https://doi.org/10.1038/s41592-020-0731-1

Punjani, A., Rubinstein, J. L., Fleet, D. J., & Brubaker, M. A. (2017). cryoSPARC: Algorithms for rapid unsupervised cryo-EM structure determination. *Nature Methods*, *14*, 290–296. https://doi.org/10.1038/nmeth.4169

Quistgaard, E. M., Low, C., Guettou, F., & Nordlund, P. (2016). Understanding transport by the major facilitator superfamily (MFS): Structures pave the way. *Nature Reviews Molecular Cell Biology*, *17*, 123–132. https://doi.org/10.1038/nrm.2015.25

Rajgopal, A., Edmondnson, A., Goldman, I. D., & Zhao, R. (2001). SLC19A3 encodes a second thiamine transporter ThTr2. *Biochimica et Biophysica Acta (BBA)-Molecular Basis of Disease*, *1537*, 175–178. https://doi.org/10.1016/S0925-4439(01)00073-4

Sabe, V. T., Ntombela, T., Jhamba, L. A., Maguire, G. E. M., Govender, T., Naicker, T., & Kruger, H. G. (2021). Current trends in computer aided drug design and a highlight of drugs discovered via computational techniques: A review. *European Journal of Medicinal Chemistry*, *224*, 113705. https://doi.org/10.1016/j.ejmech.2021.113705

Timm, D. E., Liu, J., Baker, L. J., & Harris, R. A. (2001). Crystal structure of thiamin pyrophosphokinase. *Journal of Molecular Biology*, *310*, 195–204. https://doi.org/10.1006/jmbi.2001.4727

Tylicki, A., Lotowski, Z., Siemieniuk, M., & Ratkiewicz, A. (2018). Thiamine and selected thiamine antivitamins - biological activity and methods of synthesis. *Bioscience Reports*, *38*, BSR20171148. https://doi.org/10.1042/BSR20171148

Vora, B., Green, E. A. E., Khuri, N., Ballgren, F., Sirota, M., & Giacomini, K. M. (2020). Drug-nutrient interactions: Discovering prescription drug inhibitors of the thiamine transporter ThTR-2 (SLC19A3). *The American Journal of Clinical Nutrition*, *111*, 110–121. https://doi.org/10.1093/ajcn/nqz255

Wang, J., Wang, J., Han, X., Liu, Z., Ma, Y., Chen, G., Zhang, H., Sun, D., Xu, R., Liu, Y., Zhang, Y., Wen, Y., Bao, X., Chen, Q., & Fang, F. (2021). Report of the largest Chinese cohort with SLC19A3 gene defect and literature review. *Frontiers in Genetics*, *12*, 683255. https://doi.org/10.3389/fgene.2021.683255

Waterhouse, A., Bertoni, M., Bienert, S., Studer, G., Tauriello, G., Gumienny, R., Heer, F. T., de Beer, T. A. P., Rempfer, C., Bordoli, L., Lepore, R., & Schwede, T. (2018). SWISS-MODEL: Homology modelling of protein structures and complexes. *Nucleic Acids Research*, *46*, W296–W303. https://doi.org/10.1093/nar/gky427

Wen, A., Zhu, Y., Yee, S. W., Park, B. I., Giacomini, K. M., Greenberg, A. S., & Newman, J. W. (2023). The impacts of Slc19a3 deletion and intestinal SLC19A3 insertion on thiamine distribution and brain metabolism in the mouse. *Metabolites*, *13*, 885. https://doi.org/10.3390/metabo13080885

Xia, A., Yong, X., Zhang, C., Lin, G., Jia, G., Zhao, C., Wang, X., Hao, Y., Wang, Y., Zhou, P., Yang, X., Deng, Y., Wu, C., Chen, Y., Zhu, J., Tang, X., Liu, J., Zhang, S., Zhang, J., … Yang, S. (2023). Cryo-EM structures of human GPR34 enable the identification of selective antagonists. *Proceedings of the National Academy of Sciences*, *120*, e2308435120. https://doi.org/10.1073/pnas.2308435120

Yu, J., Liao, P. J., Keller, T. H., Cherian, J., Virshup, D. M., & Xu, W. (2024). Ultra-large scale virtual screening identifies a small molecule inhibitor of the Wnt transporter Wntless. *iScience*, *27*, 110454. https://doi.org/10.1016/j.isci.2024.110454

Zeng, W. Q., Al-Yamani, E., Acierno, J. S. Jr., Slaugenhaupt, S., Gillis, T., MacDonald, M. E., Ozand, P. T., & Gusella, J. F. (2005). Biotin-responsive basal ganglia disease maps to 2q36.3 and is due to mutations in *SLC19A3*. *American Journal of Human Genetics*, *77*, 16–26. https://doi.org/10.1086/431216

Zhang, Q., Zhang, Y., Diamond, S., Boer, J., Harris, J. J., Li, Y., Rupar, M., Behshad, E., Gardiner, C., Collier, P., Liu, P., Burn, T., Wynn, R., Hollis, G., & Yeleswaram, S. (2014). The Janus kinase 2 inhibitor fedratinib inhibits thiamine uptake: A putative mechanism for the onset of Wernicke's encephalopathy. *Drug Metabolism and Disposition*, *42*, 1656–1662. https://doi.org/10.1124/dmd.114.058883

Zhao, R., & Goldman, I. D. (2013). Folate and thiamine transporters mediated by facilitative carriers (SLC19A1-3 and SLC46A1) and folate receptors. *Molecular Aspects of Medicine*, *34*, 373–385. https://doi.org/10.1016/j.mam.2012.07.006

SUPPORTING INFORMATION

Additional supporting information can be found online in the Supporting Information section at the end of this article.

How to cite this article: Gabriel, F., Windshügel, B., & Löw, C. (2025). Structure-based discovery of thiamine uptake inhibitors. *British Journal of Pharmacology*, *182*(22), 5611–5626. https://doi.org/10.1111/bph.70133